

Deconfinement of Spinons on Critical Points: Multi-Flavor $\text{CP}^1 + \text{U}(1)$ Lattice Gauge Theory in Three Dimensions

Shunsuke Takashima and Ikuo Ichinose

Department of Applied Physics, Nagoya Institute of Technology, Nagoya, 466-8555 Japan

Tetsuo Matsui

Department of Physics, Kinki University, Higashi-Osaka, 577-8502 Japan

(November 21, 2018)

In this paper, we study the three-dimensional (3D) N_f -flavor CP^1 model (a set of N_f CP^1 variables) coupled with a dynamical compact $\text{U}(1)$ gauge field by means of Monte-Carlo simulations. This model is relevant to 2D $s = 1/2$ quantum spin models, and has a phase transition line which separates an ordered phase of global spin symmetry from a disordered one. From a gauge theoretical point of view, the ordered phase is a Higgs phase whereas the disordered phase is a confinement phase. We are interested in the gauge dynamics just on the critical line, in particular, whether a Coulomb-like deconfinement phase is realized there. This problem is quite important to clarify low-energy excitations in certain class of quantum spin models. If the gauge dynamics is in the deconfinement phase there, spinons, which transform in the fundamental representation of the $\text{SU}(N_f)$ symmetry, appear as low-energy excitations. By Monte-Carlo simulations, we found that the “phase structure” on the *criticality* strongly depends on the value of N_f . For small N_f , the confinement phase is realized, whereas the deconfinement phase appears for sufficient large $N_f \geq 14$. This result strongly suggests that compact QED_3 is in a deconfinement phase for sufficiently large number of flavors of massless fermions.

I. INTRODUCTION

Some recent experiments of strongly-correlated electron systems indicate that the usual Fermi liquid theory breaks down in certain cases, and the low-energy quasi-excitations carrying fractional/exotic quantum number appear there. The fractional quantum Hall effect (FQHE)¹ is a typical example, in which composite fermions appear as relevant excitations. Another example may be quantum spin models in low spatial dimensions, which have been studied quite intensively. For certain class of $s = \frac{1}{2}$ anti-ferromagnetic (AF) spin models in two dimensions, it is argued that low-energy excitations at a quantum phase transition point are spinons^{2,3}.

For studying the above “deconfined critical point” and the quantum phase transition itself, gauge theory is quite useful. Concept of confinement and deconfinement in the gauge theory is suitable for understanding the change of particle picture happening at deconfined critical points.

In the previous paper³, we showed that the phase transition from the Néel state to the dimer state in the AF magnet corresponds to a Higgs (deconfinement) to confinement phase transition in the simple CP^1 model. There we were also interested in the gauge dynamics at the critical point. If the three-dimensional (3D) Coulomb-like phase is realized there as a simple loop expansion predicts, quasi-excitations are massless spinons. As the low-energy excitations are magnons (spin waves) in the Néel state and spin-triplet excitations in the dimer state, the existence of spinons at the criticality indicates breakdown of the traditional Ginzburg-Landau (GL) theory of phase transition. This is because the GL theory

uses an (a set of) order parameter to describe both a phase transition by its expectation value and low-energy excitations by its fluctuations in space and time.

To study the gauge dynamics of a class of spin models in a more general framework, we introduced the 3D $\text{CP}^1 + \text{U}(1)$ lattice gauge theory in Ref.⁴. The model contains two parameters, the spin stiffness c_1 and the gauge coupling c_2 , and describes the $\text{O}(3)(\text{CP}^1)$ and $\text{O}(4)$ spin models in the specific limits, ($c_2 = 0$ and $c_2 = \infty$, respectively). However, from the calculation of both instanton density and gauge-boson mass, we concluded there that the *confinement phase* is realized on its critical line⁵.

In this paper, we continue to study the gauge dynamics of these spin systems defined in two spatial dimensions at zero temperature by generalizing the above 3D $\text{CP}^1 + \text{U}(1)$ model to the 3D multi-flavor $\text{CP}^1 + \text{U}(1)$ model. In particular, we explore the possibility of change of particle picture on the criticality by controlling the flavor number N_f as an adjustable parameter.

The rest of the paper is organized as follows. In Sect.2, we explain the model and its relation to the AF Heisenberg model. In Sect.3, results of Monte-Carlo simulations are shown. We calculated the specific heat, the gauge-boson mass, and the instanton density for various values of N_f , and found that the deconfinement phase is realized on the critical line for sufficiently large N_f . Section 4 is devoted for conclusion.

II. MULTI-FLAVOR CP¹ + U(1) MODEL ON THE 3D LATTICE

Let us first define the model on the cubic lattice, and explain its relation to quantum spin models. Hereafter we use x as the site index and $\mu = 1, 2, 3$ as the direction index. On each site x , we put N_f -flavor CP¹ variables z_x^α , where α is the flavor index and takes $\alpha = 1, \dots, N_f$. z_x^α is a two-component complex field,

$$z_x^\alpha \equiv \begin{pmatrix} z_{x1}^\alpha \\ z_{x2}^\alpha \end{pmatrix}, \quad z_{x1}^\alpha, z_{x2}^\alpha \in \mathbf{C}, \quad (2.1)$$

satisfying the so-called CP¹ constraint,

$$\bar{z}_x^\alpha z_x^\alpha = \sum_{a=1,2} |z_{xa}^\alpha|^2 = 1 \quad \text{for each } x \text{ and } \alpha. \quad (2.2)$$

On each link $(x, x + \mu)$ we put a U(1) gauge variable, $U_{x\mu} = \exp(i\theta_{x\mu})$ [$\theta_{x\mu} \in (-\pi, +\pi)$]. The action of the model S is given as

$$S = -\frac{c_1}{2} \sum_{x,\mu,a,\alpha} \left(\bar{z}_{x+\mu,a}^\alpha U_{x\mu} z_{xa}^\alpha + \text{H.c.} \right) - \frac{c_2}{2} \sum_{x,\mu < \nu} \left(\bar{U}_{x\nu} \bar{U}_{x+\nu,\mu} U_{x+\mu,\nu} U_{x\mu} + \text{H.c.} \right), \quad (2.3)$$

where c_1 and c_2 are real parameters of the model. It is obvious that the action (2.3) has a local U(1) gauge symmetry as well as SU(2) and SU(N_f) global symmetries;

$$z_{xa} \rightarrow z'_{xa} = \exp(i\Lambda_x) z_{xa}, \quad U_{x\mu} \rightarrow U'_{x\mu} = \exp(i\Lambda_{x+\mu}) U_{x\mu} \exp(-i\Lambda_x), \quad (2.4)$$

$$z_{xa}^\alpha \rightarrow (z'_{xa}^\alpha)' = \sum_{b=1}^2 V_{ab} z_{xb}^\alpha, \quad V \in \text{SU}(2), \quad (2.5)$$

$$z_{xa}^\alpha \rightarrow (z'_{xa}^\alpha)' = \sum_{\beta=1}^{N_f} W^{\alpha\beta} z_{xa}^\beta, \quad W \in \text{SU}(N_f). \quad (2.6)$$

Hereafter we call the above SU(2)(SU(N_f)) symmetry the spin symmetry (flavor symmetry). The partition function Z is given by

$$Z = \int [dU]_{\text{U}(1)} [dz]_{\text{CP}^1} \exp(-S). \quad (2.7)$$

There are many gauge-invariant quantities composed of z_x^α and $U_{x\mu}$. Among them, typical *local* combinations are a set of N_f O(3) (real three-component) spins \mathbf{n}_x^α ,

$$\mathbf{n}_x^\alpha = \bar{z}_x^\alpha \boldsymbol{\sigma} z_x^\alpha, \quad \mathbf{n}_x^\alpha \cdot \mathbf{n}_x^\alpha = 1, \quad (2.8)$$

where $\boldsymbol{\sigma} = (\sigma_1, \sigma_2, \sigma_3)^t$ are the Pauli matrices. For $N_f = 1$, the model reduces in the limit of $c_2 = 0$ to the O(3) spin model described by the field \mathbf{n}_x with nearest-neighbor interactions⁴. For $N_f > 1$, there are other local gauge invariant objects $\vec{M}_x^{\alpha\beta}$, which are *four-component* O(4) vectors,

$$\vec{M}_x^{\alpha\beta} = \frac{1}{\sqrt{2}} (\bar{z}_x^\alpha \sigma_1 z_x^\beta, \bar{z}_x^\alpha \sigma_2 z_x^\beta, \bar{z}_x^\alpha \sigma_3 z_x^\beta, \bar{z}_x^\alpha z_x^\beta)^t, \quad \vec{M}_x^{\alpha\beta*} \cdot \vec{M}_x^{\alpha\beta} = 1, \quad \vec{M}_x^{\beta\alpha} = \vec{M}_x^{\alpha\beta*}. \quad (2.9)$$

$\vec{M}_x^{\alpha\beta}$ are complex for $\alpha \neq \beta$, while $\vec{M}_x^{\alpha\alpha}$ are real. In the limit of $c_2 = 0$, one can integrate over $U_{x\mu}$ link by link to obtain

$$Z_{c_2=0} = \int [dz]_{\text{CP}^1} \exp \left[\sum_{x,\mu} \log I_0(\gamma_{x\mu}) \right], \quad \gamma_{x\mu}^2 = \frac{c_1^2}{4} \sum_{\alpha,\beta=1}^{N_f} \vec{M}_{x+\mu}^{\alpha\beta} \cdot \vec{M}_x^{\beta\alpha} + \text{H.c.} \quad (2.10)$$

where $I_0(\gamma_{x\mu})$ is the modified Bessel function. We note that $\vec{M}_x^{\alpha\beta}$ are *not* all independent, so one needs to include extra interactions associated with the change of variables from z_{xa}^α to $\vec{M}_x^{\alpha\beta}$ to treat them as independent O(4) complex spin vectors. For finite c_2 , the model involves non-local and/or nonpolynomial interactions among $\vec{M}_x^{\alpha\beta}$.

On the other hand, in the limit of $c_2 \rightarrow \infty$, the gauge configuration is restricted to $U_{x\mu} = 1$ up to gauge transformations (2.4). Then the model reduces to an ensemble of *independent* N_f O(4) nonlinear sigma models,

$$Z_{c_2=\infty} = \int [dR]_{\text{O}(4)} \exp(c_1 \sum_{x,\mu,\alpha} \vec{R}_{x+\mu}^\alpha \cdot \vec{R}_x^\alpha), \quad [dR]_{\text{O}(4)} = \prod_{x,\alpha} \prod_{k=1}^4 dR_{xk}^\alpha \prod_{x,\alpha} \delta(\vec{R}_x^\alpha \cdot \vec{R}_x^\alpha - 1), \quad z_{x1}^\alpha = R_{x1}^\alpha + iR_{x2}^\alpha, \quad z_{x2}^\alpha = R_{x3}^\alpha + iR_{x4}^\alpha, \quad (2.11)$$

where \vec{R}_x^α is a four-component real O(4) vector, $\vec{R}_x^\alpha = (R_{x1}^\alpha, \dots, R_{x4}^\alpha)^t$.

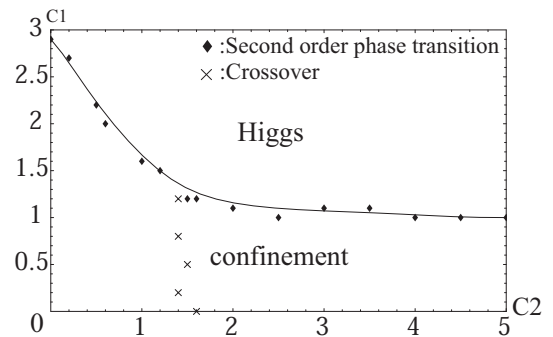


FIG. 1. Phase structure of the 3D CP¹ + U(1) model ($N_f = 1$) in the c_1 - c_2 plane obtained by the measurement of the specific heat⁴. The Higgs and confinement phases correspond to the Néel and dimer state of the quantum spin model, respectively

In the previous paper⁴, we investigated the phase structure of the $N_f = 1$ model and found that there exist two phases, the ordered phase of the symmetry (2.5) and

the disordered phase which are separated by the second-order transition line $c_1 = c_{1c}(c_2)$. (See Fig.1.) These two phases correspond to the Higgs and the confinement phases in the U(1) gauge dynamics, respectively. In the ordered phase $c_1 > c_{1c}$, there is a nonvanishing “spin magnetization” $\langle \bar{z}_x \boldsymbol{\sigma} z_x \rangle \neq 0$, and as a result the low-energy excitations are the massless components of z_{xa} , which corresponds to the spin waves in the AF magnets (see later discussion). On the other hand, in the disordered phase $c_1 < c_{1c}$, the confinement phase is realized, and the low-energy excitations are the “spin-triplet” vector field which is nothing but the composite field, $\mathbf{n}_x = \bar{z}_x \boldsymbol{\sigma} z_x$. Just on the critical line $c_1 = c_{1c}$, there is no spontaneous symmetry breaking of the internal spin symmetry and z_{xa} ($a = 1, 2$) behave as gauge-interacting massless bosons. Thus one may naturally expect that a 3D Coulomb-like phase with a potential $1/r$ may be realized there because of the screening effect by the massless bosons z_{xa} . In such a phase on the critical line, the low-energy excitations are to be “weakly interacting massless spinons” z_{xa} . With this possibility in mind, we studied the gauge dynamics on the critical line, and found that *the confinement phase is realized there*. This result means that the CP¹ model coupled with the dynamical gauge field (2.3) belongs to the same universality class as the O(3) nonlinear σ model.

The $N_f = 1$ case of the CP¹ model (2.3) is known to be a low-energy effective field theory of the nonuniform $s = \frac{1}{2}$ AF Heisenberg model on a square lattice^{3,6,7},

$$H_{AF} = \sum_{x,j} J_{xj} \hat{S}_x \cdot \hat{S}_{x+j} + \dots, \quad (2.12)$$

where j is the spatial direction index ($j = 1, 2$), \hat{S}_x is the quantum spin operator at site x , and J_{xj} is the nonuniform exchange coupling. (See Fig.2.) The ellipses in Eq.(2.12) represent other multi-spin interactions. By varying the couplings J_{xj} , the *ground state* of the Hamiltonian

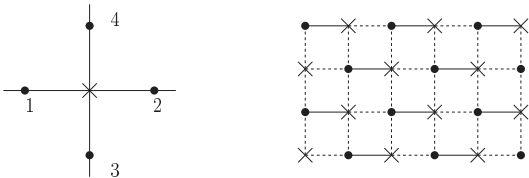


FIG. 2. 2D square lattice; crosses are odd sites, and filled circles are even sites. Solid bonds indicate that their exchange couplings are stronger than those on the dotted bonds.

(2.12) changes from the Néel state to the dimer state⁸. In the Néel state, there exists an AF long-range order and the low-energy excitations are the spin waves. On the other hand, the ground state of the dimer state consists of spin-singlet pairs on nearest-neighbor (NN) sites, and low-energy excitations are the spin-triplets. (See Fig.3.)

The quantum spin operator \hat{S}_x is expressed by the Schwinger boson, i.e., the CP¹ boson operator, as follows;

$$\hat{S}_x = \frac{1}{2} z_x^\dagger \boldsymbol{\sigma} z_x, \quad (2.13)$$

and the CP¹ constraint, $\sum_a z_{xa}^\dagger z_{xa} |\text{phys}\rangle = |\text{phys}\rangle$, restricts the magnitude of the spin to $\frac{1}{2}$. It was shown that the above Néel-dimer phase transition is nothing but the transition of the CP¹ model discussed above³. Therefore our investigation on the critical behavior of the CP¹ model⁴ indicates that the *quantum* phase transition in the system (2.12) belongs to the *same universality class* with the *classical* phase transition in the 3D O(3) nonlinear σ model⁹.

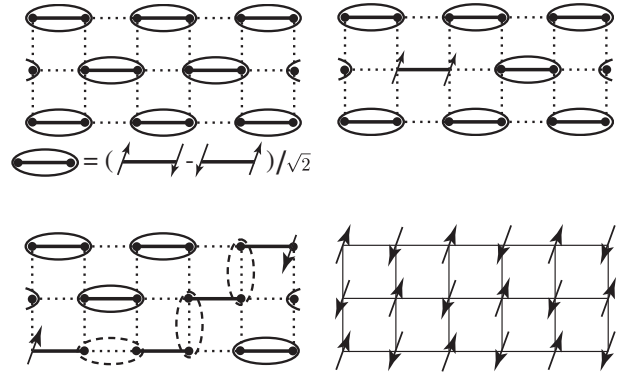


FIG. 3. Ground states and excitations of the nonuniform AF Heisenberg model of Eq.(2.12). Each arrow represents one of the two spinon states $z_x = (1, 0)^t$ and $z_x = (0, 1)^t$. Each oval represents a singlet pair of NN spins. (a) dimer state, (b) spin-triplet excitation in the dimer state, (c) two-spinon state having the energy proportional to their distance (confinement phenomenon), (d) Néel state with an AF long-range order.

The above result supports the traditional idea for quantum phase transition that a *quantum* system in d spatial dimensions belongs to the same universality class of a certain *classical* system in $d + z$ dimensions, where z is called dynamical critical exponent¹⁰. In recent years, however, it has been recognized that the above idea of the dynamical exponent breaks down in some cases; non-trivial physics appears at the criticality of *quantum* phase transitions. The spinons, as it was explained above, are a typical example of such interesting possibility.

In order to see the above interesting phenomenon of quantum phase transition, we shall extend the model. The CP^N model in the 3D continuum space-time is certainly such a model, which can be studied by the $1/N$ expansion¹¹. In the leading order of the $1/N$, a nontrivial infrared fixed point appears. On this fixed point, i.e., on the critical point, a nonlocal term for the gauge field $A_\mu(x)$ like,

$$N \int d^3x \int d^3y \sum_{\mu,\nu} F_{\mu\nu}(x) \frac{1}{|x-y|^2} F_{\mu\nu}(y),$$

$$F_{\mu\nu} = \partial_\mu A_\nu - \partial_\nu A_\mu, \quad (2.14)$$

appears in the effective action due to the vacuum polarization of the massless z_x . At long distances, the above

term dominates the usual Maxwell term which may exist in the original action. From (2.14), it is straightforward to calculate the potential energy $V(r)$ between the two charges separated by a distance r as $V(r) \propto 1/r$. Then it is quite interesting to study the CP^N models on the lattice for various values of N , in particular, to investigate the change in their critical behaviors.

Below we shall study the multi-flavor CP^1 model (2.3) numerically instead of the CP^N model. The reason to choose the multi-flavor CP^1 model is simply a matter of simplicity and shorter computing time in Monte-Carlo simulations. In the large- N limit, it is expected that the both models exhibit similar behavior.¹²

III. NUMERICAL RESULTS

In this section, we present the results of our numerical study of the model on the 3D cubic lattice of the system size $N = L^3$, $L = 8, 12, 16$ with the periodic boundary condition for the flavor number $N_f = 1, 2, 3, 4, 5, 10, 14$, and 18. We measured the internal energy, the specific heat, the mass of the gauge boson, and the instanton density. We observed no hysteresis in the internal energy $\langle S \rangle / N$.

A. Specific heat

We first show the results of the specific heat $C \equiv \langle (S - \langle S \rangle)^2 \rangle / N$ measured in order to determine the phase structure.

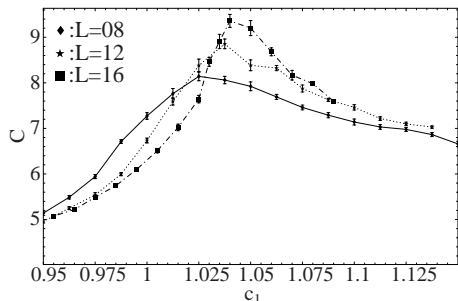


FIG. 4. Specific heat C vs. c_1 at $c_2 = 2.0$ for the $N_f = 2$ case. The system size is $8^3, 12^3$ and 16^3 . C shows typical behavior of the second-order phase transition.

In Fig.4 and Fig.5 we present C at the gauge coupling $c_2 = 2.0$ for $N_f = 2$ and 14, respectively. These results show a typical behavior of the second-order phase transition. To confirm the transition is of second-order, we fit these data by the finite-size scaling hypothesis (FSSH)¹³. To this end, we introduce a parameter $\epsilon \equiv (c_1 - c_{1\infty})/c_{1\infty}$ where $c_{1\infty}$ is the critical coupling in the infinite system ($L \rightarrow \infty$). Then we assume that the correlation length at $L \rightarrow \infty$ scales as $\xi \propto \epsilon^{-\nu}$ with a critical exponent ν . We also assume that the maximum of C at $L \rightarrow \infty$, C_∞

diverges as $C_\infty \propto \epsilon^{-\sigma}$ with another exponent σ . Then FSSH predicts that the specific heat $C_L(\epsilon)$ for the system size L scales as

$$C_L(\epsilon) = L^{\sigma/\nu} \phi(L^{1/\nu} \epsilon), \quad (3.1)$$

where $\phi(x)$ is the scaling function¹³. The scaling function obtained from the data in Fig.5 is shown in Fig.6. The parameters are estimated as $\nu = 1.0, c_{1\infty} = 1.01$ and $\sigma = 0.20$. The function $\phi(x)$ is well determined, and it is obvious that the FSSH is satisfied quite well. We investigated the phase structure of the CP^N ($N = 2, 3, 4$) models and also $N_f = 2, 3$ cases of the multi-flavor CP^1 models by calculating the specific heat. We conclude that the phase structures of both the multi-flavor $CP^1+U(1)$ model and the $CP^N+U(1)$ model are similar to that of the $CP^1+U(1)$ model shown in Fig.1.

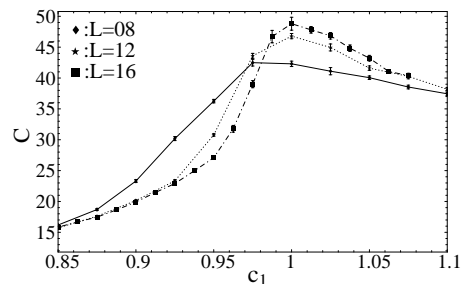


FIG. 5. Specific heat C vs. c_1 at $c_2 = 2.0$ for the $N_f = 14$ case.

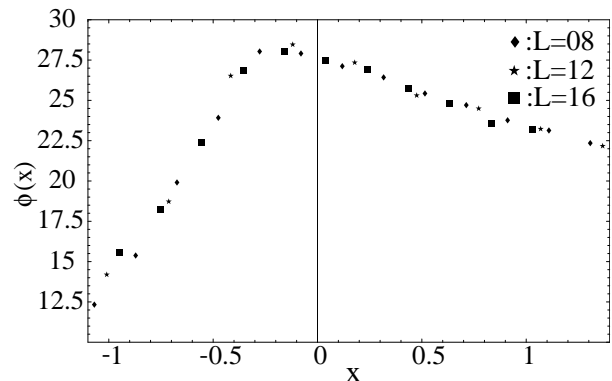


FIG. 6. Finite-size scaling function $\phi(x)$ of Eq.(3.1) determined by using C of Fig.5. All the data of $L = 8, 12$ and 16 are fitted well by the single function $\phi(x)$.

B. Mass of gauge boson

Now let us turn to the gauge-boson mass. We calculate the gauge-invariant gauge-boson mass M_G as follows^{4,14}. To define M_G we first introduce a gauge-invariant operator $O(x)$,

$$\begin{aligned}
O(x) &= \sum_{\mu,\nu=1,2} \epsilon_{\mu\nu} \text{Im} (\bar{U}_{x\nu} \bar{U}_{x+\nu,\mu} U_{x+\mu,\nu} U_{x\mu}) \\
&= \sum_{\mu,\nu} \epsilon_{\mu\nu} \sin(-\theta_{x\nu} - \theta_{x+\nu,\mu} + \theta_{x+\mu,\nu} + \theta_{x\mu}), \quad (3.2)
\end{aligned}$$

where $\epsilon_{\mu\nu}$ is the antisymmetric tensor. Then we introduce the Fourier transformed field $\tilde{O}(x_3)$ as follows,

$$\tilde{O}(x_3) = \sum_{x_1, x_2} O(x) e^{ip_1 x_1 + ip_2 x_2}. \quad (3.3)$$

We define the gauge correlation function,

$$D_G(t) = \frac{1}{L^3} \sum_{x_3} \langle \tilde{O}(x_3) \bar{\tilde{O}}(x_3 + t) \rangle. \quad (3.4)$$

In the continuum, $D_G(t)$ is expected to behave as

$$\begin{aligned}
D_G(t) &= \int dp_3 \frac{e^{ip_3 t}}{p^2 + M_G^2} \\
&\propto e^{-\sqrt{p_1^2 + p_2^2 + M_G^2} t}. \quad (3.5)
\end{aligned}$$

Typical behavior of the correlator $D_G(t)$ is shown in Fig.7. We determine M_G by fitting the data $D_G(t)$ by the exponential form (3.5). For practical calculations, we set $p_1 = p_2 = 2\pi/L$.

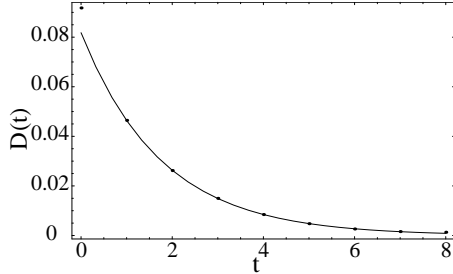


FIG. 7. Gauge correlation function $D_G(t)$ of Eq.(3.4) for $N_f = 18$ at $c_1 = 0.90$ and $c_2 = 2.0$ with $L = 16$.

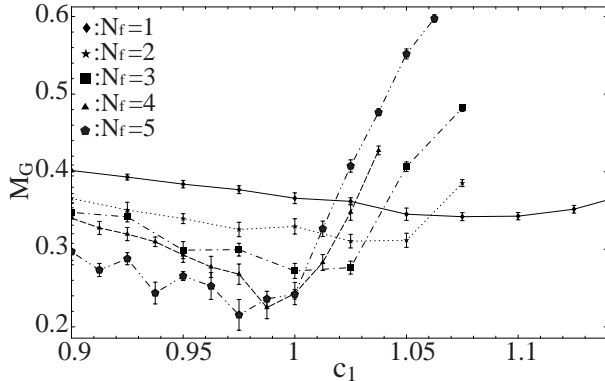


FIG. 8. Gauge-boson mass M_G vs. c_1 at $c_2 = 2.0$ for $N_f = 1, \dots, 5$. M_G do not vanish for these N_f 's.

In Fig.8 and Fig.9, we plot M_G for $N_f = 1 \sim 5$ and $N_f = 10, 14, 18$, respectively. From the results in Fig.8, it is obvious that the gauge-boson mass has the minimum in the region close to the phase transition. The minimum of the value of M_G decreases as N_f increases as expected, but it is still nonvanishing. In the previous paper⁴, we observed similar behavior of M_G in the $CP^N + U(1)$ model for $N = 1, 2, 3, 4$.

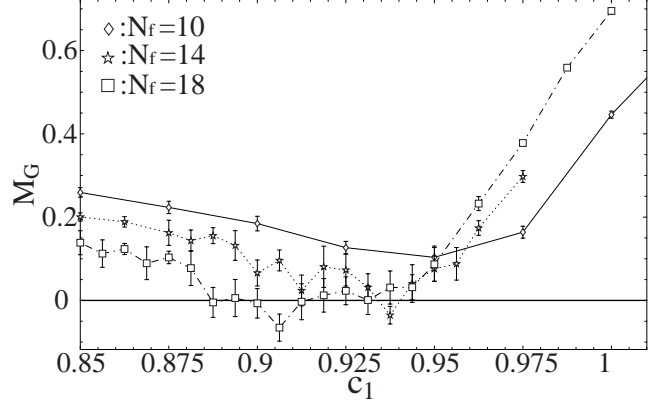


FIG. 9. Gauge-boson mass M_G vs. c_1 at $c_2 = 2.0$ for $N_f = 10, 14$ and 18 . The data show that M_G vanishes in the critical region for $N_f = 14$ and 18 . The case of $M_G < 0$ implies that the square of exponent of Eq.(3.5), $\gamma \equiv M_G^2 + p_1^2 + p_2^2$ is smaller than $2(2\pi/L)^2$ and we defined $M_G \equiv -[2(2\pi/L)^2 - \gamma]^{1/2}$.

On the other hand, M_G for $N_f = 10, 14, 18$ in Fig.9 shows that M_G vanishes at the criticality for $N_f \geq 14$. This indicates that a deconfinement phase is realized on the critical line for large N_f . Appearance of the deconfinement phase stems from the shielding effect by the massless bosons z_x^α . On the critical line, low-energy excitations are massless z_x^α and massless gauge boson $\theta_{x\mu}$. Furthermore, we expect that topological nontrivial excitations, i.e., instantons, become irrelevant on the critical line due to a large number of the massless z_x^α . (See later discussion.)

From the data of Fig.8 and Fig.9, one can locate the minimum value of M_G along the line $c_2 = 2.0$ for each N_f . These minima are presented in Fig.10. The minimum value of M_G seems to decrease continuously as N_f increases. By making the linear extrapolation of the data for $N_f = 1 \sim 5$ and 10 , we estimate that M_G starts to vanish at $N_f \simeq 13.5$. This value is regarded as the critical flavor number at which the phase on the criticality changes continuously from the confinement phase to the deconfinement Coulomb-like phase.

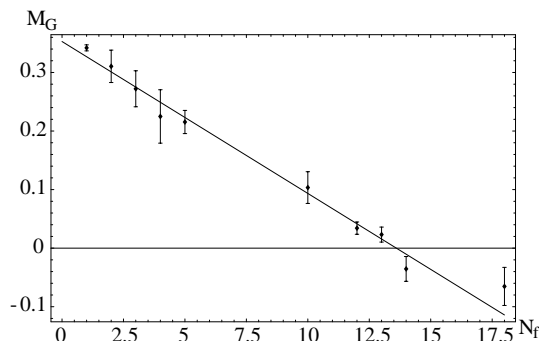


FIG. 10. The minimum value of gauge-boson mass M_G for $c_2 = 2.0$ vs. the flavor number N_f . The straight line interpolates the data for $N_f = 1 \sim 5, 10$, which intercepts $M_G = 0$ at $N_f = 13.54$.

C. Instantons

Instantons play an important role in compact U(1) gauge theories¹⁵. Their proliferation (condensation) enhances fluctuations of U(1) gauge field and induces the confinement phase of the gauge dynamics. In the present 3D case, the instantons are just the magnetic monopoles and their condensation puts the system into the “dual” superconducting phase. The dual Meissner effect squeezes electric fluxes one-dimensionally, and as a result a pair of oppositely charged point particles separated by a distance r have the energy proportional to r , i.e., they are confined.

In order to measure the instanton density, let us define instanton charge as in Ref.¹⁶. The magnetic flux $\Theta_{x,\mu\nu}$ penetrating plaquette $(x, x + \mu, x + \mu + \nu, x + \nu)$ is given as,

$$\Theta_{x,\mu\nu} \equiv \theta_{x\mu} + \theta_{x+\mu,\nu} - \theta_{x+\nu,\mu} - \theta_{x\nu}, \quad (-4\pi < \Theta_{x,\mu\nu} < 4\pi). \quad (3.6)$$

We decompose $\Theta_{x,\mu\nu}$ into its *integer* part $2\pi n_{x,\mu\nu}$ ($n_{x,\mu\nu}$ is an integer) and the remaining part $\tilde{\Theta}_{x,\mu\nu} \equiv \Theta_{x,\mu\nu} \pmod{2\pi}$,

$$\Theta_{x,\mu\nu} = 2\pi n_{x,\mu\nu} + \tilde{\Theta}_{x,\mu\nu}, \quad (-\pi < \tilde{\Theta}_{x,\mu\nu} < \pi). \quad (3.7)$$

Physically, $n_{x,\mu\nu}$ describes the Dirac string. The instanton charge Q_x at the cube around the dual site $\tilde{x} = x + (\hat{1} + \hat{2} + \hat{3})/2$ is defined as

$$\begin{aligned} Q_x &= -\frac{1}{2} \sum_{\mu,\nu,\rho} \epsilon_{\mu\nu\rho} (n_{x+\mu,\nu\rho} - n_{x,\nu\rho}) \\ &= \frac{1}{4\pi} \sum_{\mu,\nu,\rho} \epsilon_{\mu\nu\rho} (\tilde{\Theta}_{x+\mu,\nu\rho} - \tilde{\Theta}_{x,\nu\rho}), \end{aligned} \quad (3.8)$$

where $\epsilon_{\mu\nu\rho}$ is the complete antisymmetric tensor. Then it is obvious that Q_x measures the total flux emanating from the monopole(instanton) sitting at \tilde{x} . The instanton density ρ is defined as

$$\rho = \sum_x |Q_x|/N. \quad (3.9)$$

In Fig.11, we show the instanton density ρ at $c_2 = 2.0$ as a function c_1 for the $N_f = 1$ and $N_f = 18$ cases. As snapshots of instanton configurations in Ref.⁴ show, some of instantons form pairs with anti-instantons located at NN sites, i.e., instanton-anti-instanton dipoles. These dipoles are not effective for disordering the gauge-field dynamics and do not contribute to confinement. In fact, the confinement phase of the gauge dynamics is nothing but the plasma phase of the instantons as first shown by Polyakov¹⁷. On the other hand, the insulating phase of the instantons, in which almost all instantons form dipoles, is the deconfinement phase of the gauge dynamics. Then the density of *isolated (single)* instantons is a physical quantity which monitors whether the system is in the (de)confinement phase. Therefore in Fig.11, we also show the density of isolated instantons ρ_{is} ,

$$\rho_{is} \equiv \rho - 2\rho_{dp}, \quad (3.10)$$

where ρ_{dp} is the density of NN instanton-anti-instanton dipoles defined similarly as in Eq.(3.9) (The factor 2 in front of ρ_{dp} in Eq.(3.10) comes from the fact that a dipole is composed of an instanton and an anti-instanton).

In Fig.11, both ρ and ρ_{is} almost vanish for $c_1 > c_{1c}$ in the $N_f = 18$ case in which M_G vanishes at the critical point. However, in the $N_f = 1$ case, there remains a finite instanton density at the critical point. This result and the calculation of M_G indicate that the Coulomb phase is realized on the critical line for $N_f \geq 14$.

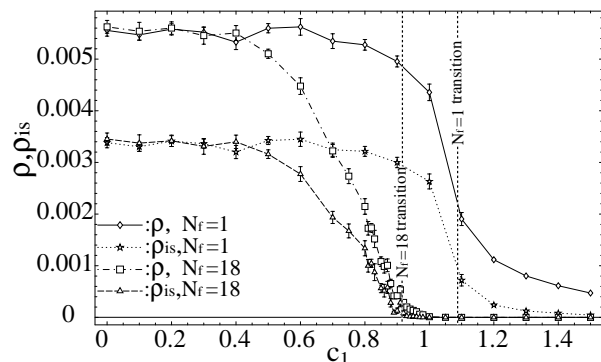


FIG. 11. Density of instantons ρ and that of isolated instantons ρ_{is} at $c_2 = 2.0$ vs. c_1 for $N_f = 1$ and $N_f = 18$. It is obvious that both ρ and ρ_{is} for $N_f = 18$ tend to vanish for $c_1 \geq c_{1c}$, whereas ρ and ρ_{is} for $N_f = 1$ remain finite at the critical point.

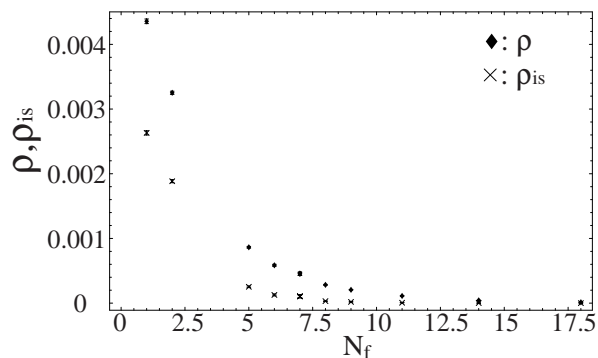


FIG. 12. Instanton densities ρ and ρ_{is} at $c_2 = 2.0$ and $c_1 = 1.0$ as a function of N_f .

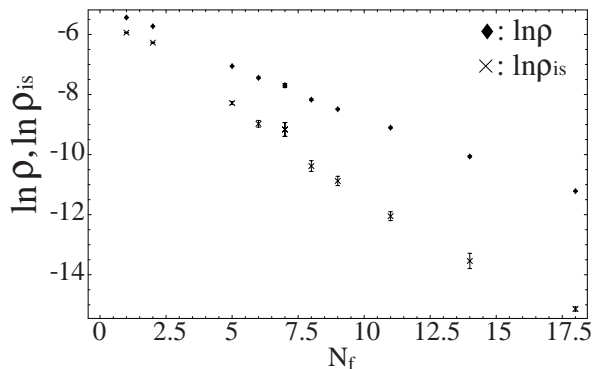


FIG. 13. Log-plot of instanton densities ρ and ρ_{is} at $c_2 = 2.0$ and $c_1 = 1.0$ as a function of N_f . It is obvious that $\ln \rho$, $\ln \rho_{is} \propto (-N_f)$.

It is interesting to see how the instanton density changes as a function of the flavor number N_f . Results are shown in Figs.12 and 13 for $c_1 = 0.1$ and $c_2 = 2.0$. From the results, it is obvious that ρ scales as $\rho \propto e^{-AN_f}$ for $N_f \geq 5$, where A is a certain constant. This means that the main contribution in the effective gauge theory comes from the vacuum polarization of z_{xa}^α ($\alpha = 1, \dots, N_f$, $a = 1, 2$). In fact the effective gauge theory $S_{\text{eff}}(U)$ obtained by integrating out the CP^1 variables in Eq.(2.7) has the following form,

$$Z = \int [dU]_{\text{U}(1)} \exp(-S_{\text{eff}}), \quad (3.11)$$

where

$$S_{\text{eff}} = N_f S_z - \frac{c_2}{2} \sum_{x,\mu < \nu} \left(\bar{U}_{x\nu} \bar{U}_{x+\nu,\mu} U_{x+\mu,\nu} U_{x\mu} + \text{H.c.} \right),$$

$$\exp(-S_z) = \int [dz] \exp \left(\frac{c_1}{2} \sum_{x,\mu,a,\alpha} (\bar{z}_{x+\mu,a}^\alpha U_{x\mu} z_{xa}^\alpha + \text{H.c.}) \right). \quad (3.12)$$

In Eq.(3.12), $\int [dz]$ denotes the integral over *single* CP^1 field. From the above form of $S_{\text{eff}}(U)$, it is expected

that $S_z(U)$ dominates over the single-plaquette term for sufficiently large N_f and it determines the constant A in the fitting ρ as actually observed in Fig.13.

IV. CONCLUSION

In this paper we studied the multi-flavor CP^1 model in three dimensions by Monte-Carlo simulations. In particular, we are interested in the gauge dynamics on the critical line which separates the Higgs (Néel) and confinement (dimer) phases. On the critical line, “spinons” z_x^α are massless. Their fluctuations shield the confining gauge force at least partly. If the number of these spinons is sufficiently large, the confining forces may be completely shielded by them and the deconfining (Coulomb-like) force may appear instead. By calculating the gauge-boson mass and the instanton density, we found that the Coulomb-like deconfinement phase is actually realized for $N_f \geq 14$. The low-energy excitations on the critical line are the massless “spinons” z_x^α and massless gauge boson. Similar deconfinement phase is expected to appear on the critical points of the large- N solution of the CP^N model.

As far as the shielding phenomenon is concerned, massless fermions give a similar effect as massless bosons. Thus the present result indicates that the parity-preserving QED_3 with massless four-component-spinor fermions should have a deconfinement phase for sufficiently large flavor number of fermions, as long as the chiral symmetry is *not* spontaneously broken to avoid the generation of the dynamical mass. For example, in perturbation theory, gauge-interacting fermions generate the nonlocal terms like Eq.(2.14). Recently, 3D $\text{U}(1)$ gauge theories coupled with gapless matter fields have been studied quite intensively, in particular, to answer the question whether a confinement-deconfinement phase transition takes place¹⁸. The results of the present paper are in agreement with those obtained in these works.

One may wonder how the results in this paper are applied to the dynamics of realistic quantum spin models. The corresponding quantum model for the N_f -flavor CP^1 model is the $\text{SU}(2) \times \text{SU}(N_f)$ “spin” AF magnets, whereas for the CP^N model that is $\text{SU}(N+1)$ “spin” AF magnets. Unfortunately, as far as we know, there are no materials which have the above internal quantum degrees of freedom. However, as we explained in the introduction and also in the above, study of the strongly-correlated electron systems often reduces to the study of certain gauge models of gapless matter fields. The results in the present paper should give an important insight into the phase structures of these gauge systems and the related strongly-correlated electron systems.

- ¹ R.Laughlin, Phys.Rev.Lett.50, 1395(1983); D.Haldane, Phys.Rev.Lett.51, 605(1983); J.K.Jain, Phys.Rev.Lett.63, 199(1989).
- ² T.Senthil, V.Vishwanath, L.Balents, S.Sachdev, and M.P.A.Fisher, Science 303, 1490(2004); T.Senthil, L.Balents, S.Sachdev, V.Vishwanath, and M.P.A.Fisher, Phys.Rev.B70, 144407(2004).
- ³ D.Yoshioka, G.Arakawa, I.Ichinose, and T.Matsui, Phys.Rev.B77, 174407(2004).
- ⁴ S.Takashima, I.Ichinose, and T.Matsui, Phys.Rev.B72, 075112(2005).
- ⁵ The discrepancy between the two alternative results for the Néel-dimer critical point of the 2D AF Heisenberg spin model, the deconfinement phase³ or the confinement phase⁴, implies that the inverse effective gauge-coupling constant g_1 was overestimated in Ref.³. g_1 should be *below* the critical coupling g_c to put the system in the confinement phase to agree with Ref.⁴.
- ⁶ I.Ichinose and T.Matsui, Phys.Rev.B45, 9976(1992).
- ⁷ D.P.Arovas and A.Auerbach, Phys.Rev.B38, 316(1988).
- ⁸ P.Tomczak and J.Richter, J.Phys.A34, L461(2001), and references cited therein.
- ⁹ T.Senthil, L.Balents, S.Sachdev, A.Vishwanath, and M.P.A.Fisher, J.Phys.Soc.Jpn.74, Suppl.1(2005); However see also, B.A.Bernevig, D.Giuliano, and R.B.Laughlin, Annals Phys.311, 182(2004); Ki-Seok Kim, Phys.Rev.B72, 035109(2005).
- ¹⁰ See for example, D.Belitz, T.R.Kirkpatrick, and T.Vojta, Rev.Mod.Phys.77, 579(2005).
- ¹¹ I.Ya.Aref'eva and S.I.Azakov, Nucl.Phys.B162, 298(1980); A.D'Adda, P.Di Vecchia and M. Lüscher, Nucl.Phys.B146, 63(1978); E.Witten, Nucl.Phys.B149, 285(1979).
- ¹² Here we assume that the $SU(N_f)$ symmetry (2.6) is *not* spontaneously broken.
- ¹³ See, for example, J.M.Thijssen, "*Computational Physics*" (Cambridge University Press, 1999).
- ¹⁴ K.Kajantie, M.Karjalainen, M.Laine, and J.Peisa, Phys.Rev.B57, 3011(1998).
- ¹⁵ See for example, S.Coleman, "*Aspect of Symmetry*" (Cambridge University Press, 1985).
- ¹⁶ T.A.DeGrand and D.Toussaint, Phys.Rev.D22, 2478(1980).
- ¹⁷ A.M.Polyakov, Nucl.Phys.**B120**, 429(1977); For the Abelian Higgs model in 3D, see S.Wenzel, E.Bittner, W.Janke, A.M.J.Schakel, and A.Schiller, Phys.Rev.Lett.**95**, 051601(2005).
- ¹⁸ See for example, H.Kleinert, F.S.Nogueira, and A.Sudbø, Phys.Rev.Lett.88, 232001(2002); Nucl.Phys.B666, 361(2003); F.S.Nogueira and H.Kleinert, Phys.Rev.Lett.95, 176406(2005); G.Arakawa, I.Ichinose, T.Matsui, and K.Sakakibara, Phys.Rev.Lett.94, 211601(2005); G.Arakawa, I.Ichinose, T.Matsui, K.Sakakibara and S.Takashima, Nucl.Phys.B732, 401(2006); S.Takashima, I.Ichinose, T.Matsui, and K.Sakakibara, hep-lat/0511010, and references cited therein.